Desalination and Water Treatment
www.deswater.com

doi: 10.5004/dwt.2023.29289

284 (2023) 288–300
February

Adsorption of methylene blue onto activated carbon prepared under N_2/microwave radiation supported cobalt: kinetics, isotherms, and thermodynamics studies

Fedia Mechati[a], Chahrazed Djilani[b,*], Nabil Bougdah[b], Nabil Messikh[b], Elhadi Boussaha[b], Abdelhak Moumen[b], Chafia Bouchalta[a], Mohamed Salah Medjram[a]

[a]*Laboratory LGCES, Faculty of Technology, University 20 August 1955, El-Hadaeik Road, P.O. Box: 26, Skikda, Algeria, emails: f.mechati_26@hotmail.com (F. Mechati), cbouchelta2000@yahoo.fr (C. Bouchalta), medjram_ms@yahoo.fr (M.S. Medjram)*
[b]*Faculty of Technology, University 20 August 1955, El-Hadaeik Road, P.O. Box: 26, Skikda, Algeria, emails: chahrazed_dj@yahoo.fr (C. Djilani), Bougdah_nabil@yahoo.fr (N. Bougdah), nabchem@yahoo.fr (N. Messikh), bhedi3@yahoo.fr (E. Boussaha), abdo_moumen@yahoo.fr (A. Moumen)*

Received 12 May 2022; Accepted 9 January 2023

ABSTRACT

This study aims to investigate the kinetics, isotherms, and thermodynamics of methylene blue (MB) dye adsorption from aqueous solution onto activated carbon prepared from orange peel waste (PO). This material was chemically treated with sulfuric acid, pyrolyzed, and activated in microwave apparatus under nitrogen flow. The resulting activated carbon was supported using cobalt transition metal by a wet impregnation process at different cobalt (Co) contents; the optimum condition was achieved at cobalt impregnations of 20 wt.%. The supported carbon Co20 wt.%-POAC catalyst was characterized by scanning electron microscopy, Fourier-transform infrared spectroscopy, and Brunauer–Emmett–Teller surface area analysis. The results show that the equilibrium was reached at 270 min with an adsorption capacity of 27 $mg \cdot g^{-1}$; the Langmuir isotherm was the best model that describes the experimental data. Besides, the pseudo-first-order adsorption model best depicts the adsorption kinetics of the MB by Co20 wt.%-POAC. Thermodynamic analysis shows that the standard Gibb's free energy change ($\Delta G°$) has negative values, confirming, therefore, the feasibility and spontaneity of the process. The changes in enthalpy ($\Delta H°$) and entropy ($\Delta S°$) were found to be –2,011 $J \cdot mol^{-1}$ and18.9 $J \cdot K^{-1} \cdot mol^{-1}$, respectively. Finally, our results revealed that grafting cobalt onto the surface of the orange peel-activated carbon improves its adsorption capacity, and hence its efficiency in removing MB from wastewater.

Keywords: Activated carbon; Microwaves activation; Orange peel; Cobalt catalysts; Adsorption; Kinetic; Thermodynamic; Equilibrium isotherm.

1. Introduction

The needs to protect aquatic environments are very high due to increased industrialization that reduces the availability of clean water. Polluted water is of great concern to aquatic organisms, plants, and humans [1]. Particularly, the extensive use of dyes in many industries around the world has led to a variety of environmental issues related to polluted waters, such as preventing the penetration of sunlight and reducing the photosynthetic activity of

* Corresponding author.

streams [2], inducing harmful impacts on fish and other aquatic organisms. Among dyes, methylene blue (MB) is one of the most used organic dyes [3] for dyeing cotton, wood, and silk [4]. It is characterized by a high molecular weight and a complex chemical structure, making it toxic and carcinogenic [5] due to its non-biodegradability [6]. The treatment of colored effluents before discharge into public water sources is therefore important. To salvage the aquatic environment, several physical and chemical methods are available, such as advanced oxidation [7], ultrafiltration, photodegradation [8], and coagulation–flocculation [9]. The adsorption process has been successfully used as one of the most effective techniques to treat water environments [10,11]. Owing to its superior adsorption capacity when compared with other adsorbents, activated carbon is the most recommended adsorbent for dye removal [12]. Agricultural solid waste and biomass have received increasing attention as precursors for the activated carbon production, they are cost-effective, sustainable, and widespread [13,14]. Moreover, they require a reduced processing time and can be easily regenerated [15].

Commonly, activated carbon is produced and modified by physical and chemical methods to enhance its adsorption capacities by modifying its surface and internal porous structure [16,17]. The preparation of activated carbon under microwave radiation has recently received much attention due to the several advantages over conventional heating methods such as rapid and uniform heating [18,19], energy saving, and reduced processing time [20,21]. Microwave heating is commonly used for the synthesis and pyrolysis of chemical substances [22–25].

The use of activated carbons supported by transition metals (Fe, Co, Ni, Cu, etc.), acting simultaneously as adsorbents [26,27] and catalysts [28,29] has proven to be effective for dye removal. This efficiency is mainly related to their high specific surface area, porous structure, surface functional groups, and pore size distribution [30,31]. Due to its magnetic properties, high activity, and selectivity, cobalt has been used in the synthesis of supported activated carbons for the degradation of dyes [32,33].

The aim of this work is focused on the synthesis and preparation of adsorbents and catalysts from biomaterials that may reduce the activation time and improve the adsorption capacity. For this purpose, an agricultural waste was used to produce an activated carbon adsorbent. Few studies in the literature were carried out on the use of metal-supported activated carbons produced from agricultural wastes, including rice straw [34], tea waste [35], date pits [36], sea-buckthorn stones [37] as catalysts in the field of wastewater treatment and environmental protection.

In this investigation, the adsorbent was prepared from orange peel and modified by pyrolysis, then activated by microwave heating and grafted on its surface with cobalt (Co) using the impregnation method.

The different materials (PO, POAC, Co-POAC) were characterized using scanning electron microscopy (SEM), Fourier-transform infrared spectroscopy (FTIR), and Brunauer–Emmett–Teller (BET) analyses. The effect of different parameters such as contact time and adsorbent dosage on the removal of MB from aqueous solutions under the optimum conditions of impregnation rates of cobalt was investigated. The performance of Co20 wt.%-POAC on MB adsorption was evaluated using kinetic and thermodynamic studies. In addition, adsorption isotherms were determined and modeled.

2. Materials and methods

2.1. Preparation of activated carbon

Orange peel (PO) was first washed with distilled water to eliminate impurities (dust and water–soluble substances), then dried at 110°C for 24 h to remove the water until reaching a constant weight. After, it was milled in a Muller and sieved into a uniform size of less than 2.0 mm.

The precursor was all chemically activated with 40% solution of H_2SO_4 (in a ratio of 1 g of precursor per 4 mL of solution). The mixture of the material and the activating agent was stirred for 10 min at room temperature, then boiled and stirred for 3 h. The solution was placed in an oven at 120°C for 24 h. The solid obtained by filtration was washed several times with hot and cold distilled water, respectively until a neutral pH was reached. Finally, the material was dried in an oven at 110°C for at least 12 h.

The obtained product was pyrolyzed under nitrogen flow in a horizontal tubular furnace (length of 450 mm and internal diameter of 65 mm). The reactor is a quartz tube (750 mm length and 35 mm internal diameter), placed into the furnace. Two thermocouples were used for both temperature measurement and furnace monitoring. In this stage, about 10 g of the precursor was placed in the middle of the reactor at 400°C pyrolysis temperature, 100 $cm^3 \cdot min^{-1}$ of nitrogen flow, and a heating rate of 10°C min^{-1}. Once the pyrolysis temperature was reached, the sample was maintained at this temperature for another 1 h. The resulting char was activated with microwave radiation under nitrogen flow, then placed in a ceramic crucible, and put into a commercial microwave oven (Procombi Whirlpool MOD. AVM 840/WP/GR) with the frequency of 2.45 GHz and purged with nitrogen flow at about 300 $cm^3 \cdot min^{-1}$ flow rate. The activation step was performed at a microwave power of 600 W, and 3 min of irradiation [38]. The obtained activated carbon was denoted POAC.

2.2. Impregnation of the support

The obtained material was impregnated using an aqueous solution of cobalt(II) nitrate hexahydrate CoN_2O_6, $6H_2O$ with different proportions (5, 10, 15, and 20 wt.%), then we added 40 mL of distilled water and ethanol (75% distilled water and 25% ethanol). After, the pH was neutralized to 11 by NaOH (1 M) with magnetic stirring for 24 h at ambient temperature, and then ultrasonicated for 2 h to obtain complete penetration and saturation of the metal ions in the activated carbon pores [27]. After the evaporation of the solvent and the washing of the catalyst precursor, several times with distilled water until a neutral pH was obtained, it was then dried in an oven at 110°C for about 24 h. Finally, the obtained samples were calcined under nitrogen (N_2) flow at 400°C for 1 h. Catalysts were named Co5 wt.%-POAC, Co10 wt.%-POAC, Co15 wt.%-POAC and Co20 wt.%-POAC.

To determine the efficiency of the activated carbon-supported cobalt catalyst, we tested its efficiency for the removal of methylene blue from an aqueous solution.

2.3. Characterization methods

Thermogravimetric analysis (TGA/DTG) allows continuous recording of sample mass changes with linearly increasing temperature. The apparatus used was a 2050 TGA V5.4A (TA Instruments). The thermal evolution of raw materials was followed by thermogravimetric analysis (TGA) from room temperature up to 600°C. The sample to be analyzed had a mass of approximately 20 mg.

The microstructure and morphology of PO, POAC, and Co20 wt.%-POAC were examined using a scanning electron microscope (HITACHI S-2360 N) with a magnification range of 300–3,000, and an acceleration voltage range of 20–22 kV.

FTIR was employed to identify the functional groups present at the surface of the different samples. The spectra were recorded in the frequency range of 650–4,000 cm^{-1} using an FTIR spectrophotometer (Spectrum One FTIR spectrometer).

The specific surface area and pore structure characteristic of POAC and Co-POAC was measured by N_2 adsorption at 77.35 K, using the BET method on a manometric sorptometer ASAP2020 (Micromeritics). The catalyst micropore volumes were calculated using the Dubinin–Radushkevich (DR) method and the specific surface area of the micropores was determined by the t-plot technique.

2.4. Adsorption experiments

2.4.1. Equilibrium adsorption studies

The equilibrium time indicates the possible diffusion control mechanism between the adsorbate as it moves toward the adsorption surface [39], it is one of the important parameters for the successful employment of the adsorbents for practical application [40]. For determining at what time the adsorption equilibrium is reached, 0.1 g of each adsorbent was put into 300 mL of methylene blue (MB) solution at the initial concentration of 10 $mg{\cdot}L^{-1}$. The amount of dyes adsorbed at time t, q_t ($mg{\cdot}g^{-1}$), was calculated by the following equation:

$$q_t = \frac{\left(C_0 - C_t\right)V}{m} \tag{1}$$

where C_o and C_t ($mg{\cdot}L^{-1}$) are MB concentrations at initial and at any time t, respectively, V is the volume of the solutions (L), and m is the mass of the used adsorbent (g).

To get the optimum adsorption conditions, the effect of adsorbent dosage on adsorption was also studied in a batch reactor at room temperature of 25°C by varying the adsorbent from 0.02 to 0.5 g with an initial dye concentration of 10 $mg{\cdot}L^{-1}$ and an initial volume of 200 mL for the corresponding contact time.

2.4.2. Adsorption isotherms

Adsorption isotherm experiments were carried out in 250 mL glass-stoppered flasks at a constant temperature (25°C), containing 0.1 g of Co20 wt.%-POAC and 100 mL dye solutions with various initial concentrations (10, 20, 40, 60, 80, 100, 200 and 300 $mg{\cdot}L^{-1}$). The flasks were agitated in an isothermal water-bath shaker at 200 rpm until the equilibrium was reached. The residual concentration of dye was determined with a double beam UV-Vis spectrophotometer (1800 SHIMADZU) at λ_{max} (665 nm). MB uptake at equilibrium, q_e (mg/g) was calculated by Eq. (2):

$$q_e = \frac{\left(C_0 - C_e\right)V}{m} \tag{2}$$

where C_o and C_e are the initial and the equilibrium concentrations of MB in the solution ($mg{\cdot}L^{-1}$), respectively, V is the total volume of solution (L) and m is the adsorbent dosage (g).

Two adsorption models (Langmuir and Freundlich) were applied to the experimental data.

The non-linear expression for the Langmuir isotherm is [41,42]:

$$q_e = q_m \frac{K_L C_e}{1 + K_L C_e} \tag{3}$$

where C_e is the equilibrium concentration of ions ($mg{\cdot}L^{-1}$), q_e is the amount of the metallic ions adsorbed ($mg{\cdot}g^{-1}$), q_m and K_L are the maximal adsorption capacity ($mg{\cdot}g^{-1}$), and the Langmuir equilibrium constant ($L{\cdot}g^{-1}$), respectively. The main characteristics of the Langmuir isotherm can be expressed by a dimensionless constant called the separation factor R_L [43].

$$R_L = \frac{1}{1 + K_L C_0} \tag{4}$$

R_L values indicate the adsorption to be unfavorable when $R_L > 1$, favorable ($0 < R_L < 1$), linear ($R_L = 1$), or irreversible when ($R_L = 0$) [44].

The Freundlich model is given by the non-linear equation:

w q_e is the amount adsorbed ($mg{\cdot}g^{-1}$), C_e is the equilibrium concentration of the adsorbate ($mg{\cdot}L^{-1}$), K_F is the Freundlich adsorption constant ($mg{\cdot}g^{-1}$), n is a parameter usually greater than unity, and related to the deviation of the isotherm from linearity.

2.4.3. Thermodynamic study

Thermodynamic parameters can be determined using the equilibrium constant K (q_e/C_e) which depends on temperature. The change in free energy ($\Delta G°$), enthalpy ($\Delta H°$) and entropy ($\Delta S°$) associated with the adsorption process was calculated using the following equations:

$$\Delta G = -RT \ln K \tag{5}$$

$$\ln K = \frac{\Delta S°}{R} - \frac{\Delta H°}{RT} \tag{6}$$

The Gibbs free energy is expressed as:

$$\Delta G^\circ = \Delta H^\circ - T\Delta S^\circ \quad (7)$$

where R is the universal gas constant (8.314 J·K^{-1}·mol^{-1}), T is the temperature (K) and K is the distribution coefficient for adsorption. ΔH° and ΔS° parameters can be calculated from the slope and intercept of the plot of ln$K$ vs. 1/T yields, respectively [45].

3. Results and discussion

3.1. Characterization

3.1.1. Thermogravimetric analyses

Fig. 1 shows the thermogravimetric analysis (TGA), and differential thermal gravimetric (DTG) curve of orange peel. TGA profile indicates that the process of weight loss contained four sections. The first weight loss of 4.8% could be due to the water evaporation, next, the decomposition peaks at the maximum temperature of 193.56°C (20.9 wt.%), 221.69°C (10.45 wt.%) and 315.14°C (31.4 wt.%) are assigned to three remaining weight loss, respectively. These results are in agreement with the literature data [46,47]. Pectin is broken between 200°C and 260°C, then hemicellulose (190°C–270°C), next cellulose (250°C–350°C), and finally lignin (270°C–500°C) [38].

3.1.2. Scanning electron microscopy

The surfaces of the different samples were observed using SEM as illustrated in Fig. 2. It can be seen that PO has an irregular and plugged porous structure. After activation, the external surface of POAC shows many cavities, indicating that the pore structure was created as a result of chemical treatment; the pore structure may have stemmed from the evaporation of the activating reagent H_2SO_4 during microwave activation, which could leave behind some void space in its place. However, after modification, the surface of Co20 wt.%-POAC became porous and smooth; this may be due to the deposition of cobalt at the surface of POAC.

3.1.3. FTIR spectra analysis

The FTIR spectra of PO, POAC, and Co-POAC are displayed in Fig. 3 while the IR absorption band assignments are collected in Table 2. The spectra of all the samples show obvious similarities. However, PO, POAC, and Co-POAC present characteristic peaks at bandwidths around 2,390 and 1,700 cm^{-1}, respectively, which could be attributed to N–H and C=O stretching vibrations, probably due to the presence of ketone groups, suggesting, the possibility of the presence of oxygen or nitrogen atoms, and carbonyl groups (C=O) [48–50].

The IR spectrum of natural precursor, PO has a characteristic peak at 3,430 cm^{-1} which is attributed to the O–H stretching vibration of the hydroxyl group, carboxylic acid, alcohol, and phenol functions; in addition, the C–O band appearing at 1,040 cm^{-1} is attributable to the ester or ether groups [50]. Thus, these observed absorption bands indicate that the functional groups such as alkene, ester, aromatic, ketone, alcohol, hydroxyl, ether, and carboxyl are present in the natural material, which is essentially composed of cellulose, hemicellulose, and lignin [51].

Furthermore, after microwave activation and cobalt impregnation, many changes have appeared in the position of the bands: the bands located at 3,430 and 1,040 cm^{-1} disappeared, and new peaks appears around 1,530 and 1,029 cm^{-1} in the FTIR spectra of Co20 wt.%-POAC, these bands were assigned to C=C stretching in the aromatic

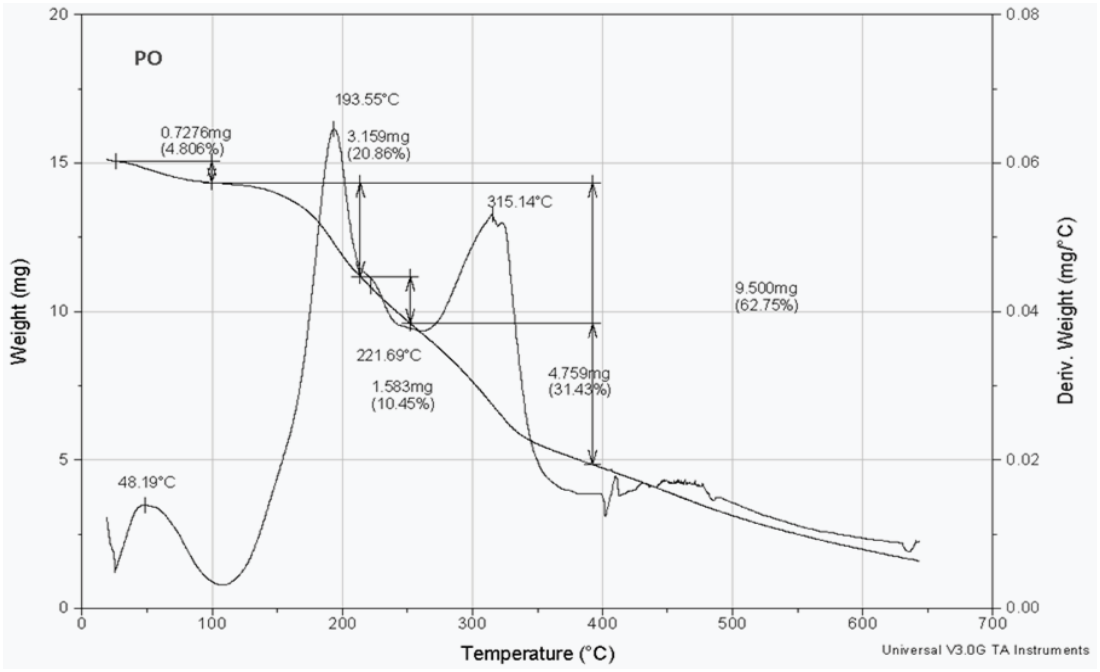

Fig. 1. TGA/DTG analysis of orange peel.

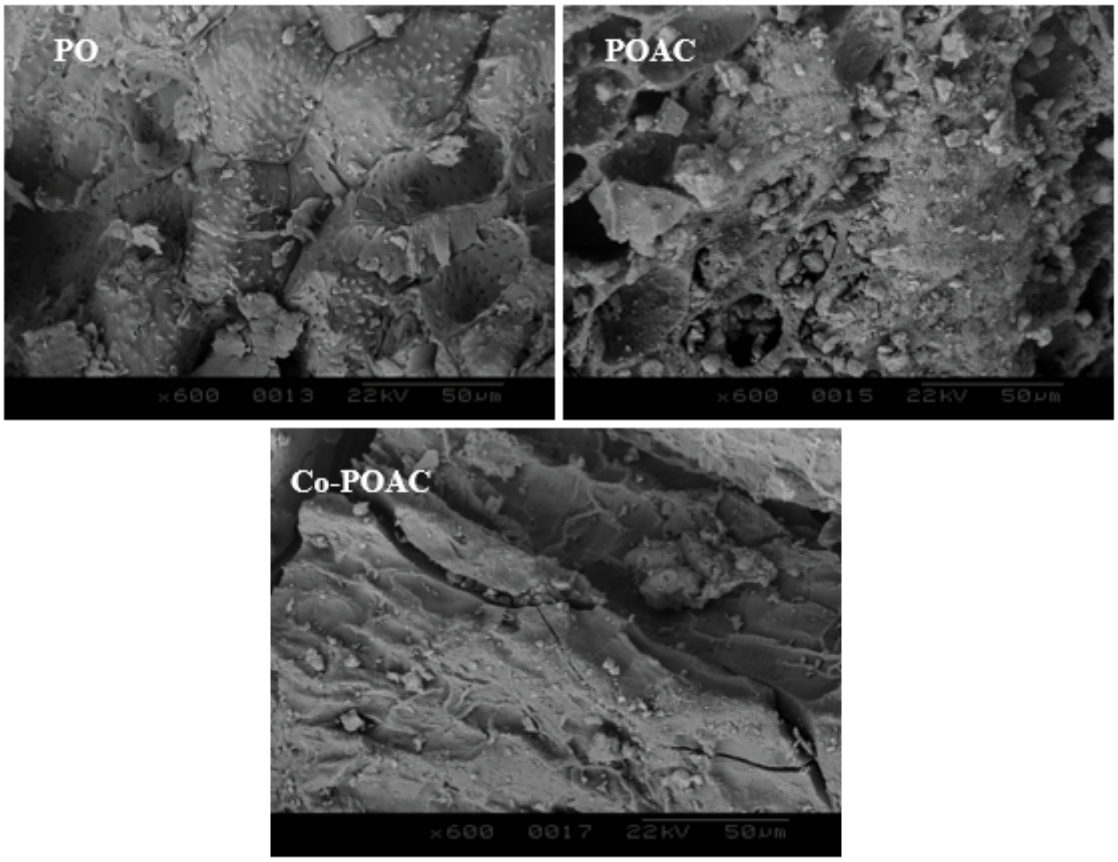

Fig. 2. SEM micrographs of PO, POAC and Co20 wt.%-POAC.

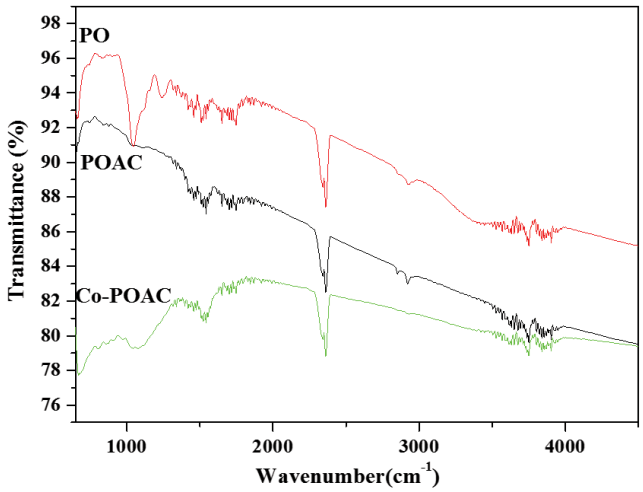

Fig. 3. FTIR spectra of PO, POAC and Co20 wt.%-POAC.

Table 1
Approximate chemical composition of PO

pH	5.57
Humidity (%)	76.43
Apparent density (g·mL^{-1})	0.19
Ash (%)	2.44

groups and the C–O stretching vibration band, respectively. These results indicate that the microwave heating method and Co-modified activated carbon reduced the content of oxygen-containing functional groups [52,53].

3.1.4. N_2 adsorption–desorption isotherms

N_2 adsorption–desorption isotherms at –196°C are shown in Fig. 4, and the texture parameters are summarized in Table 3. As shown in Fig. 4, the adsorption isotherms of both samples (POAC and Co20 wt.%-POAC) show Type I isotherm as per the IUPAC classification. All isotherms have a steep rise in the initial stage of adsorption at lower p/p_o range, there after adsorption progressed well to attain saturation at high pressure range, demonstrating its reversible single layer adsorption. The isotherms showed that the amount of N_2 adsorbed sharply increased at very low pressures, indicating a considerable development of the microporous.

According to the values presented in Table 3, the BET surface area and pore volume were found to be 408 m^2·g^{-1}; 0.218 cm^3·g^{-1} for POAC and 308 m^2·g^{-1}; 0.192 cm^3·g^{-1} for Co-POAC.

The values of the micropore area (S_{micro}) are greater than those of the external area ($S_{t\text{-}ext}$) for POAC and Co-POAC, exhibiting, therefore, Type I adsorption isotherms typical of predominant microporous structure.

The values of the microporous volume are lower than the total pore volume, which indicates the presence of a

Table 2
Assignments of IR absorption bands for PO, POAC and Co20 wt.%-POAC

Assignments	Band position (cm^{-1})		
	PO	POAC	Co20 wt.%-POAC
O–H stretching	3,430		
C–H stretching in alkyl groups	2,910	2,920	2,390
C=O stretching vibrations	2,390	2,390	1,700
C=O stretching of aldehydes, esters and ketones groups	1,710–1,693	1,900–1,700	1,530
C=C stretching of aromatic group			
C–O stretching in ester, ether, or phenol groups	1,040		1,029
C–O stretching			

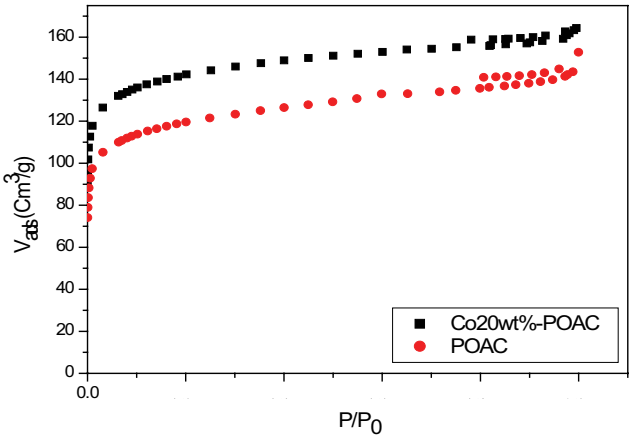

Fig. 4. N_2 adsorption–desorption isotherms at –196°C of POAC and Co20 wt.%-POAC.

non-negligible fraction of meso and macropores in the structure. Furthermore, the microporous volume and the external area value of Co-POAC are found to be lower than that of POAC, which explains the impregnation of cobalt particles onto the surface of Co-POAC. The reduction of the BET surface area of Co-POAC (308 $m^2 \cdot g^{-1}$) confirmed the good distribution of cobalt atoms, which was also verified through SEM images of POAC and Co-POAC.

3.2. Adsorption studies

3.2.1. Effect of contact time

Fig. 5 shows the effect of the contact time and the adsorption capacity of MB on the prepared samples. The series of experiments were performed with an initial concentration of MB (10 $mg \cdot g^{-1}$). The results indicate that the adsorption capacity of the different precursors increases with the increase of contact time until equilibrium is reached. It can be seen that the adsorption capacity of the activated carbon supported with cobalt is higher than that of activated carbon (POAC) and natural biomass (PO).

The system reached equilibrium after 270, 300, 330, 360, 400, and 460 min for Co20 wt.%-POAC, PO, Co15 wt.%-POAC, Co10 wt.%-POAC, Co5 wt.%-POAC, and POAC, respectively, with a maximum adsorbed amount of

Table 3
Surface pore properties of POAC and Co20 wt.%-POAC deduced from N_2 adsorption at –196°C

Samples	POAC	Co20 wt.%-POAC
S_{BET} ($m^2 \cdot g^{-1}$)	408	308
$S_{t\text{-}ext}$ ($m^2 \cdot g^{-1}$)	129.184	41.848
S_{micro} ($m^2 \cdot g^{-1}$)	279.304	262.458
Total pore volume ($cm^3 \cdot g^{-1}$)	0.218	0.192
V_{micro} ($cm^3 \cdot g^{-1}$)	0.128	0.123
Average pore diameter (Å)	10.703	25.308

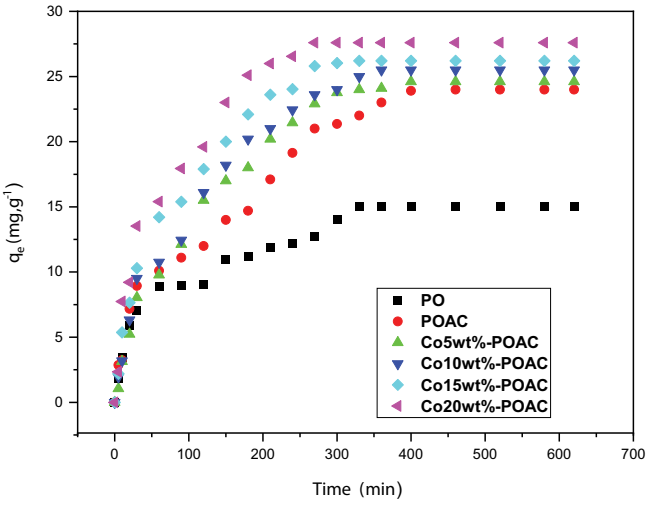

Fig. 5. Effects of contact time on adsorption capacity of (PO), (POAC), (Co5 wt.%-POAC), (Co10 wt.%-POAC), (Co15 wt.%-POAC) and (Co20 wt.%-POAC) [MB (C_o = 10 $mg \cdot L^{-1}$), T = 25°C, m all adsorbents = 0.1 g and agitation speed: 220 rpm].

15–27 $mg \cdot g^{-1}$ for all the samples. Also can be found that the adsorption capacity is classified in the following decreasing order: Co20 wt.%-POAC > Co15 wt.%-POAC > Co10 wt.%-POAC > Co5 wt.%-POAC > POAC > PO. Consequently, we consider the fast adsorption kinetics to be proportional to the high percentage of cobalt (20 wt.%) with an adsorption capacity of 27 $mg \cdot g^{-1}$; the equilibrium contact time was reached at 270 min. The low adsorption capacity is linked

to the surface modification of the activated carbon, following the occupation of the pores by the cobalt atoms.

3.2.2. Effect of adsorbent dosage

In this study, the optimization of adsorbent mass was carried out using 0.02–0.5 g of Co20 wt.%-POAC. MB concentration and contact time at room temperature were 10 mg·g^{-1} and 270 min, respectively. The results obtained from Fig. 6 indicate an increase in adsorption capacity with increasing adsorbent dose. MB adsorption increased from 71% to 92% at masses of 0.02 and 0.5 g of Co20 wt.%-POAC. Adsorption was 92% at 0.1 g and on further increasing, the mass adsorption percentage did not increase. Therefore, 0.1 g of Co20 wt.%-POAC was considered as the optimum dose. The increase in adsorption with the addition of adsorbent may be attributed to the increased number of binding sites available for MB [54]. It may be concluded that 0.1 g adsorbent mass provided sufficient adsorption sites to achieve 92% adsorption efficiency under the experimental conditions [55].

Consequently, 0.1 g of Co20 wt.%-POAC was chosen as the optimum adsorbent mass for further experiments.

3.2.3. Adsorption isotherms

Fig. 7 shows the adsorption isotherms of MB on PO, POAC, and Co20 wt.%-POAC). Initially, it is observed an increase in the adsorption, indicating an affinity between the adsorbate and the adsorbent, followed by a plateau formation that constitutes the maximum saturation for all samples. This equilibrium is established when the ratio between the adsorbed amount that remains in the solution becomes constant [30]. The adsorption isotherms were of Type I, and the maximal dye adsorption capacities determined at the plateau of isotherms are 190.791, 172.596 and 123 mg·g^{-1} for Co-POAC, POAC, and PO, respectively.

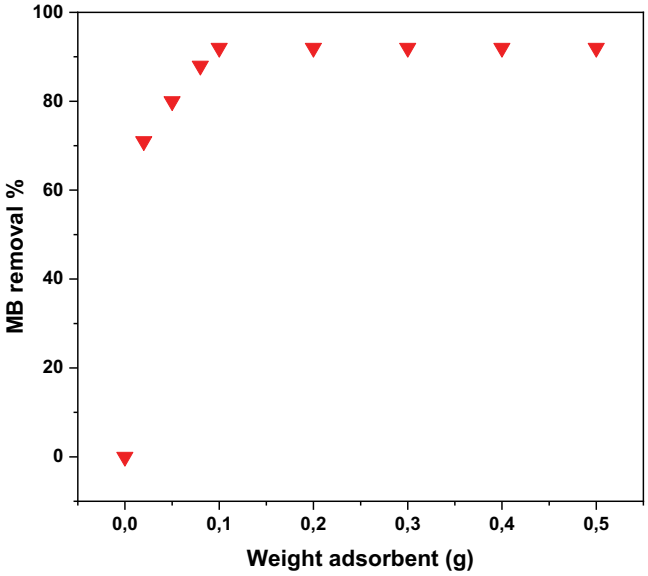

Fig. 6. Effect of adsorbent dose on the adsorption of MB by Co20 wt.%-POAC [MB (C_o = 10 mg·L^{-1}), T = 25°C and agitation speed: 220 rpm].

To fit the adsorption experimental data, Langmuir and Freundlich isotherms were used. The model parameters and correlation coefficients (R^2) are listed in Table 4. From this table, we can see that Co20 wt.%-POAC has the highest adsorption capacity with 210.743 mg·g^{-1}, followed by POAC and PO with adsorption capacities of 187.426 and 133.913 mg·g^{-1}, respectively.

From the Langmuir constant values, we observe that Co20 wt.%-POAC exhibits a higher adsorption affinity for MB than POAC and PO. For Freundlich isotherm, the n values are superior to the unit, which indicates favorable adsorption conditions and a great adsorption intensity of MB dye on all samples.

According to Fig. 7, it is clear that the Langmuir model is more suitable for describing the MB adsorption on PO, POAC, and Co20 wt.%-POAC than the Freundlich model. The comparison of correlation coefficients (R^2) of the non-linearized form of both equations indicates that the Langmuir model yields a better fit for the experimental equilibrium adsorption results. Our data were compared with the adsorption capacities of other adsorbents prepared by different methods and used for methylene blue dye adsorption. The results of this comparison are summarized in Table 5 [6,56–61].

3.2.4. Adsorption kinetics

The kinetic study is important since it describes the uptake rate of adsorbate and controls the residual time of the whole process. Several models were proposed to study the mechanisms controlling the adsorption [62]. To investigate the mechanism of adsorption of MB on Co-POAC under the optimal conditions (20%wt, 0.1 g), two kinetic models, namely, the pseudo-first-order and pseudo-second-order models were applied. These models can be expressed as:

Non-linear form of the pseudo-first-order model:

$$q_t = q_e\left(1-\exp\left(-k_1 t\right)\right) \tag{8}$$

Non-linear form of the pseudo-second-order model:

$$q_t = \frac{k_2 q_e^2 t}{\left(1+k_2 q_e t\right)} \tag{9}$$

In order to gain a deeper insight into the mechanism of adsorption, the kinetic data were treated with an intraparticle diffusion model (IPD) [63] proposed by Weber and Morris [64], according to Eq. (10):

$$q_t = Kt^{1/2} + C \tag{10}$$

where k_1 (min^{-1}) is the adsorption rate constant, k_2 (g·mg^{-1}·min^{-1}) is the rate constant of the second-order equation, K (mg·g^{-1}·min$^{-1/2}$) is the intraparticle diffusion rate constant, and C (mg·g^{-1}) is a constant that gives an idea about the thickness of the boundary layer [65].

The parameters of kinetic models are presented together in Table 6.

Table 6 shows that the correlation coefficients (R^2) of MB for the pseudo-first-order kinetics model and the

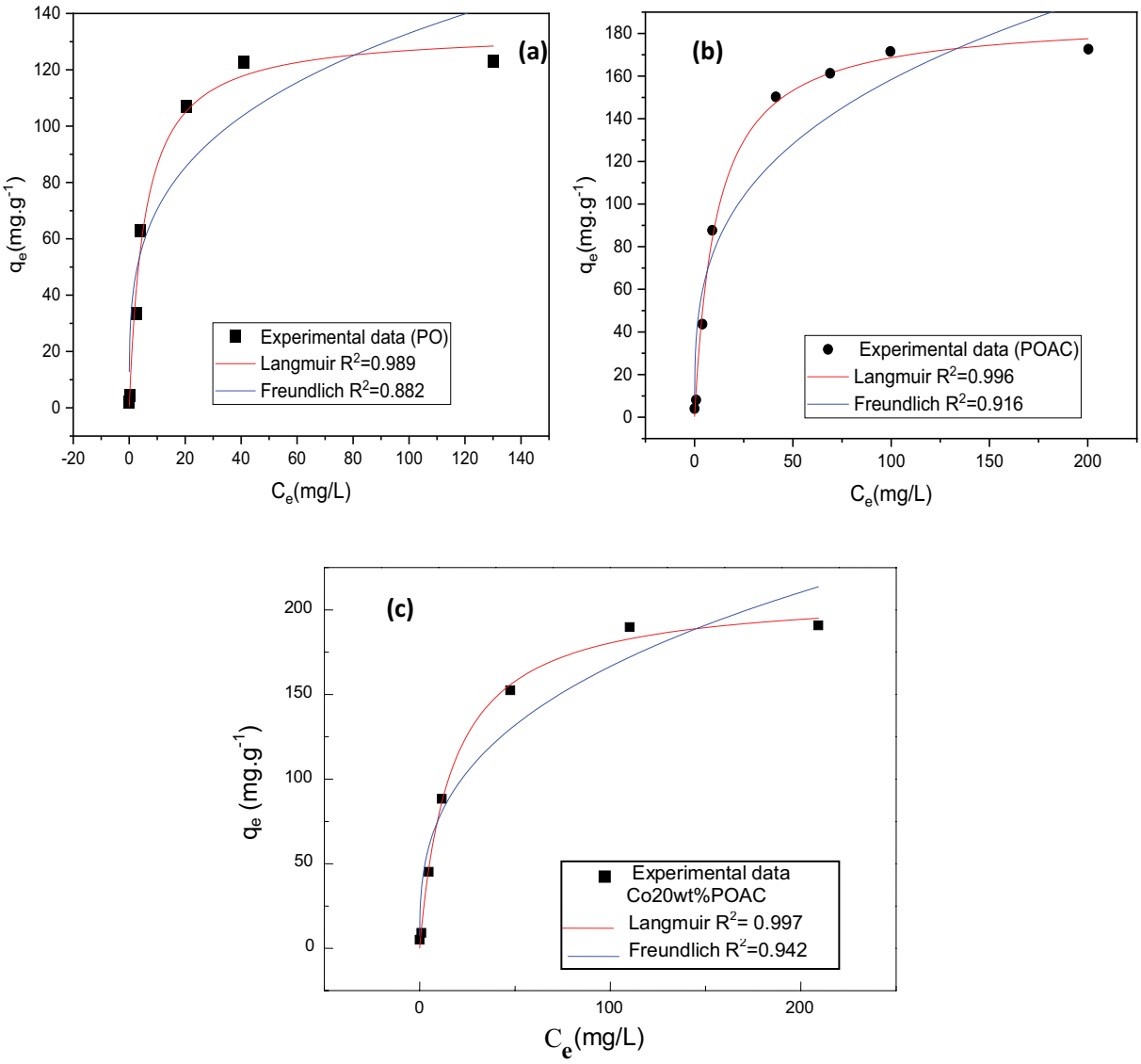

Fig. 7. Adsorption isotherms of MB on: (a) PO, (b) POAC, and (c) Co20 wt.%-POAC at 25°C [Experiments; Langmuir and Freundlich models].

Table 4
Langmuir and Freundlich parameters for MB adsorption on PO, POAC and Co20 wt.%-POAC at 25°C

	Langmuir			Freundlich		
	q_m (mg·g^{-1})	K_L	R^2	n_f	K_F	R^2
PO	133.913 ± 5.389	0.180 ± 0.030	0.988	3.627 ± 0.881	37.349 ± 19.903	0.883
POAC	187.426 ± 4.375	0.089 ± 0.009	0.996	3.274 ± 0.699	38.783 ± 11.434	0.916
Co20 wt.%-POAC	210.743 ± 4.661	0.059 ± 0.005	0.997	2.962 ± 0.529	35.187 ± 9.823	0.942

pseudo-second-order kinetics model onto Co-POAC were 0.998 and 0.990, respectively. Moreover, the adsorption capacity value q_e calculated using the pseudo-first-order model is also close to that determined by the experiment. This indicates that the pseudo-first-order adsorption model is more suitable for describing the adsorption kinetics of MB on Co20 wt.%-POAC.

However, the results obtained using the pseudo-first-order model are not enough to predict the diffusion mechanism [66]. Therefore, the intraparticle diffusion model is

investigated to analyze the adsorption kinetic data using the empirical relationship (11). A plot of q_t vs. $t^{1/2}$ should be linear if intraparticle diffusion is involved in the adsorption process and if the straight line passes through the origin, then intraparticle diffusion is the rate-controlling step. Otherwise, the adsorption process may involve some other mechanisms along with intraparticle diffusion [67]. The plot of q_t vs. $t^{1/2}$ (Fig. 9) exhibits a linear portion with a correlation coefficient of 0,990. The combined effects of film diffusion and surface reaction control [68] can explain the negative value of C (Table 6).

Table 5
Comparison of the adsorption capacity of methylene blue onto various adsorbents

Adsorbents	Dyes	Adsorption capacity ($mg·g^{-1}$)	References
Nuts shell of Argan	MB	64.62	[6]
Rice husk	MB	9.83	[56]
Banana stem date	MB	101.01	[57]
Palm leaves	MB	58.14	[58]
Graphene oxide	MB	357.14	[59]
Typha Latifolia	MB	66.67	[60]
Phragmites australis	MB	46.8	[61]
Orange peel	MB	210.74	This study

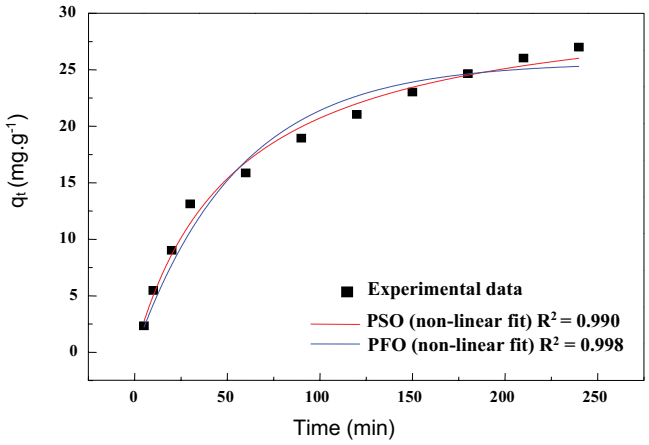

Fig. 8. Pseudo-first-order and pseudo-second-order kinetic plot for the adsorption of MB removal from aqueous solution using Co20 wt.%-POAC adsorbent (T = 25°C, m = 0.1 g and C_o = 10 mg·L^{-1}).

3.2.5. Thermodynamics studies

The effect of temperature on the phenomenon of adsorption was studied by varying this parameter from 20°C to 50°C using 300 mL of MB with 0.1 g of Co20 wt.%-POAC for 270 min at room temperature. The various thermodynamic parameters were calculated according to Eqs. (5) and (6), where $\Delta S°$ and $\Delta H°$ were obtained from the slope and intercept of the plots of $\ln K_d$ vs. $1/T$ (Fig. 10). The calculated parameters are collected in Table 7.

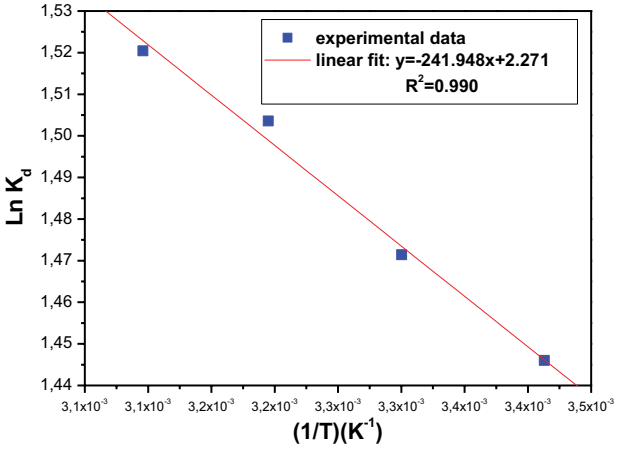

Fig. 10. Plots of $\ln K_d$ vs. $1/T$ for the adsorption of MB removal from aqueous solution using Co20 wt.%-POAC adsorbent (m = 0.1 g and C_o = 10 mg·L^{-1}).

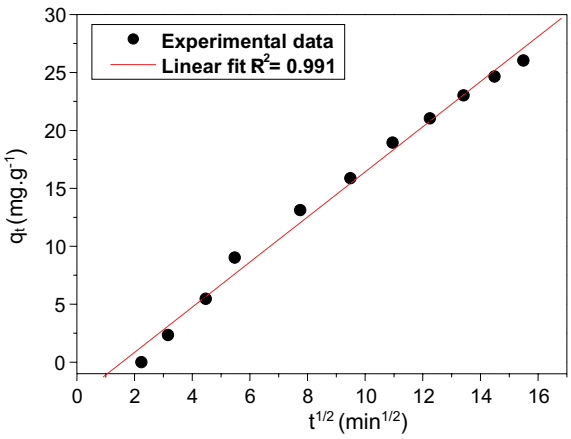

Fig. 9. Intraparticle diffusion kinetics for adsorption of the MB removal from aqueous solution using Co20 wt.%-POAC adsorbent (T = 25°C, m = 0.1 g and C_o = 10 mg·L^{-1}).

Table 6
Pseudo-first-order, pseudo-second-order and intraparticle diffusion models kinetics parameters of MB adsorption on Co20 wt.%-POAC

Pseudo-first-order			Pseudo-second-order			Intraparticle diffusion		
k_1 (min^{-1})	$q_{e,calc}$ ($mg·g^{-1}$)	R^2	k_2 ($g·mg^{-1}·min^{-1}$)	$q_{e,calc}$ ($mg·g^{-1}$)	R^2	K ($mg·g^{-1}·min^{-1/2}$)	C ($mg·g^{-1}$)	R^2
0.015 ± 0.723	26.013 ± 0.022	0.998	$5.861 \times 10^{-4} \pm 9.398 \times 10^{-5}$	31.825 ± 1.302	0.990	1.947 ± 0.061	–3.058 ± 0.623	0.990

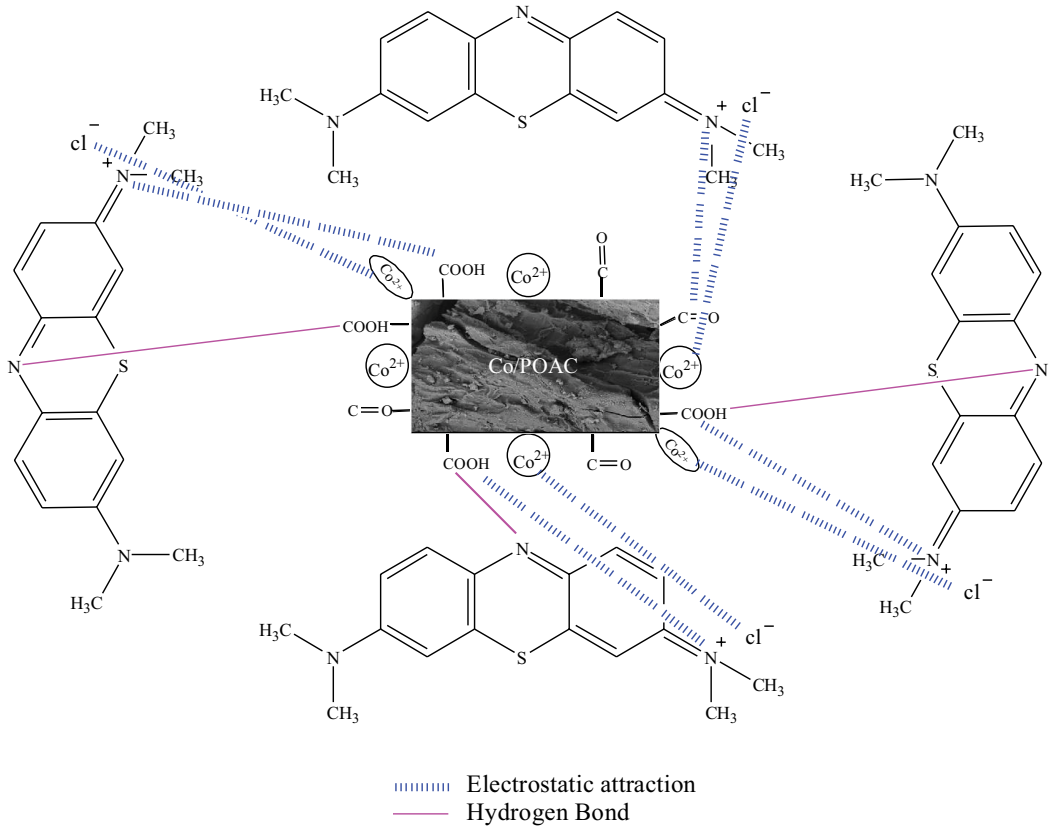

Fig. 11. Proposed adsorption mechanism of MB dye onto Co/POAC.

Table 7
Thermodynamic parameters of MB adsorption onto Co20 wt.%-POAC

Temperature (K)	$\Delta G°$ (J·mol^{-1})	$\Delta H°$ (J·mol^{-1})	$\Delta S°$ (J·K^{-1}·mol^{-1})
293	–7,540	–2,011 ± 139.6	18.9 ± 0.4
303	–7,728		
313	–7,917		
323	–8,105		

The values of enthalpy ($\Delta H°$) and entropy ($\Delta S°$) were found to be respectively –2,011 and 18.9 J·K^{-1}·mol^{-1}. Moreover, Gibbs free energy ($\Delta G°$) was –7,540; –7,728; –7,917 and –8,105 J·mol^{-1} for temperatures of 293, 303, 313, and 323 K, respectively. The negative values of $\Delta H°$ and $\Delta G°$ of the Co20 wt.%-POAC/BM system indicate the spontaneous and exothermic nature of the adsorption processes. From Table 7, $\Delta G°$ decreases with the increase in temperature, indicating an increase in the feasibility of adsorption at higher temperatures while the positive value of $\Delta S°$ shows the increasing randomness at the solid/liquid interface during the adsorption process [69].

3.3. Proposed mechanism of adsorption

According to the above experimental results, a possible mechanism for MB degradation by the Co/POAC is proposed as illustrated in Fig. 11, consisting of (i) electrostatic interaction of MB molecules with the groups of the activated carbon surface (cobalt, hydroxyl, and carboxyl), (ii) formation of hydrogen bonding between the oxygenated groups (H-donor) at the surface of the activated carbon and the amino groups (H-acceptor) of MB dye [70] and (iii) π–π interactions [71] between the aromatic rings of MB molecules and the surface of the activated carbon.

4. Conclusion

In the present work, kinetics, equilibrium, and thermodynamic studies for the adsorption of MB dye onto the activated carbon prepared under N_2/microwave radiations and supported by cobalt (Co-POAC) as a catalyst were investigated. The effect of adding cobalt on the surface of the activated carbon played a key role in the performance of the prepared catalyst by improving the adsorption kinetics of MB in an aqueous solution.

The results show that the adsorption equilibrium of MB is reached at 270 min for Co20 wt.%-POAC with an adsorption capacity of 27 mg·g^{-1}. The adsorption isotherms of MB at room temperature are well reproduced by the Langmuir model and the adsorption kinetics of MB obey the pseudo-first-order adsorption model. The thermodynamic parameters show that $\Delta H°$ and $\Delta G°$ values are negative in the temperature range of 298–323 K suggesting the spontaneous nature of the adsorption of MB onto the Co20 wt.%-POAC. The positive value of $\Delta S°$ indicates the good affinity of MB toward the Co20 wt.%-POAC and the increased

randomness at the solid-solution interface during the adsorption process.

Co-POAC has high removal efficiency than the PO and POAC systems. In a conclusion, our results demonstrated that orange-peel activated carbon prepared under N_2/microwave radiation and supported with cobalt can serve as a catalyst for the treatment of methylene blue wastewater.

References

[1] E.W. de Menezes, E.C. Lima, B. Royer, F.E. de Souza, B.D. dos Santos, J.R. Gregório, T.M.H. Costa, Y. Gushikem, E.V. Benvenutti, Ionic silica-based hybrid material containing the pyridinium group used as an adsorbent for textile dye, J. Colloid Interface Sci., 378 (2012) 10–20.

[2] S. Shakoor, A. Nasar, Removal of methylene blue dye from artificially contaminated water using citrus limetta peel waste as a very low-cost adsorbent, J. Taiwan Inst. Chem. Eng., 66 (2016) 154–163.

[3] O. Yu. Golubeva, S.V. Pavlova, Adsorption of methylene blue from aqueous solutions by synthetic montmorillonites of different compositions, Glass Phys. Chem., 42 (2016) 207–213.

[4] E. Bazrafshan, F.K. Mostafapour, M.A. Zazouli, Methylene blue (cationic dye) adsorption into *Salvadora persica* stems ash, Afr. J. Adv. Biotechnol., 11 (2012) 16661–16668.

[5] M. El Khomri, N. El Messaoudi, A. Dbik, S. Bentahar, A. Lacherai, Efficient adsorbent derived from Argania Spinosa for the adsorption of cationic dye: kinetics, mechanism, isotherm and thermodynamic study, Surf. Interfaces, 20 (2020) 100601, doi: 10.1016/j.surfin.2020.100601.

[6] A.A. Inyinbor, F.A. Adekola, G.A. Olatunji, Kinetics, isotherms and thermodynamic modeling of liquid phase adsorption of Rhodamine B dye onto *Raphia hookerie* fruit epicarp, Water Resour. Ind., 15 (2016) 14–27.

[7] A. Asghar, A.A. Abdul Raman, W.M.A. Wan Daud, Advanced oxidation processes for in-situ production of hydrogen peroxide/hydroxyl radical for textile wastewater treatment: a review, J. Cleaner Prod., 87 (2015) 826–838.

[8] E. Kordouli, K. Bourikas, A. Lycourghiotis, C. Kordulis, The mechanism of azo-dyes adsorption on the titanium dioxide surface and their photocatalytic degradation over samples with various anatase/rutile ratios, Catal. Today, 252 (2015) 128–135.

[9] Y. Al-Ani, Y. Li, Degradation of C.I. Reactive Blue 19 using combined iron scrap process and coagulation/flocculation by a novel $Al(OH)_3$–polyacrylamide hybrid polymer, J. Taiwan Inst. Chem. Eng., 43 (2012) 942–947.

[10] V.M. Vučurović, R.N. Razmovski, U.D. Miljić, V.S. Puškaš, Removal of cationic and anionic azo dyes from aqueous solutions by adsorption on maize stem tissue, J. Taiwan Inst. Chem. Eng., 45 (2014) 1700–1708.

[11] S. Agarwal, I. Tyagi, V.K. Gupta, N. Ghasemi, M. Shahivand, M. Ghasemi, Kinetics, equilibrium studies and thermodynamics of methylene blue adsorption on *Ephedra strobilacea* saw dust and modified using phosphoric acid and zinc chloride, J. Mol. Liq., 218 (2016) 208–218.

[12] S. Moosavi, C.W. Lai, S. Gan, G. Zamiri, O.A. Pivehzhani, M.R. Johan, Application of efficient magnetic particles and activated carbon for dye removal from wastewater, ACS Omega, 5 (2020) 20684–20697.

[13] J. Zhang, T. Shang, X. Jin, J. Gao, Q. Zhao, Study of chromium(VI) removal from aqueous solution using nitrogen-enriched activated carbon based bamboo processing residues, RSC Adv., 5 (2015) 784–790.

[14] H.R. Lotfy, J. Misihairabgwi, M.M. Mutwa, The preparation of activated carbon from agroforestry waste for wastewater treatment, Afr. J. *Pure* Appl. *Chem.*, 6 (2012) 149–156.

[15] M. Abbas, Performance of apricot stone to remove dyes from aqueous solutions – equilibrium, kinetics, isotherms modeling and thermodynamic studies, Mater. Today Proc., 31 (2020) 437–443.

[16] G.M. Santana, R.C.C. Lelis, J.B. Paes, R.M. Morais, C.R. Lopes, Activated carbon from bamboo (*Bambusa vulgaris*) for methylene blue removal: prediction to the environment applications, Cienc. Florestal, 28 (2018) 1179–1191.

[17] Y. Gokce, Z. Aktas, Nitric acid modification of activated carbon produced from waste tea and adsorption of methylene blue and phenol, Appl. Surf. Sci., 313 (2014) 352–359.

[18] P.N.Y. Yek, W. Peng, C.C. Wong, R.K. Liew, Y.L. Ho, W.A.W. Mahari, E. Azwar, T.Q. Yuan, M. Tabatabaei, M. Aghbashlo, C. Sonne, S.S. Lam, Engineered biochar via microwave CO_2 and steam pyrolysis to treat carcinogenic Congo red dye, J. Hazard. Mater., 395 (2020) 122636, doi: 10.1016/j.jhazmat.2020.122636.

[19] A.S. Franca, L.S. Oliveira, A.A. Nunes, C.C.O. Alves, Microwave assisted thermal treatment of defective coffee beans press cake for the production of adsorbents, Bioresour. Technol., 101 (2010) 1068–1074.

[20] W. Hu, S. Cheng, H. Xia, L. Zhang, X. Jiang, Q. Zhang, Q. Chen, Waste phenolic resin derived activated carbon by microwave-assisted KOH activation and application to dye wastewater treatment, Green Process. Synth., 8 (2019) 408–415.

[21] V.O. Njoku, K.Y. Foo, M. Asif, B.H. Hameed, Preparation of activated carbons from rambutan (*Nephelium lappaceum*) peel by microwave-induced KOH activation for acid yellow 17 dye adsorption, Chem. Eng. J., 250 (2014) 198–204.

[22] K.Y. Foo, B.H. Hameed, Utilization of oil palm biodiesel solid residue as renewable sources for preparation of granular activated carbon by microwave induced KOH activation, Bioresour. Technol., 130 (2013) 696–702.

[23] A.V. Maldhure, J.D. Ekhe, Preparation and characterizations of microwave assisted activated carbons from industrial waste lignin for Cu(II) sorption, Chem. Eng. J., 168 (2011) 1103–1111.

[24] C.H. Hsieh, S.L. Lo, W.H. Kuan, C.L. Chen, Adsorption of copper ions onto microwave stabilized heavy metal sludge, J. Hazard. Mater., 136 (2006) 338–344.

[25] S. Yuanyuan, Y. Qinyan, M. Yanpeng, G. Baoyu, G. Yuan, H. Lihui, Enhanced adsorption of chromium onto activated carbon by microwave-assisted H_3PO_4 mixed with Fe/Al/Mn activation, J. Hazard. Mater., 265 (2014) 191–200.

[26] T. Tsoncheva, I. Genov, D. Panev, M. Dimitrov, B. Tsyntsarski, N. Velino, R. Ivanova, G. Issa, D. Kovacheva, T. Budinova, I. Mitov, N. Petrov, Cobalt- and iron-based nanoparticles hosted in SBA-15 mesoporous silica and activated carbon from biomass: effect of modification procedure, Solid State Sci., 12 (2015) 1293–2558.

[27] W. Wang, X. Wang, X. Wang, L. Yang, Z. Wu, S. Xia, J. Zhao, Cr(VI) removal from aqueous solution with bamboo charcoal chemically modified by iron and cobalt with the assistance of microwave, J. Environ. Sci. (China), 25 (2013) 1726–1735.

[28] M. Iwanow, T. Gärtner, V. Sieber, B. König, Activated carbon as catalyst support: precursors, preparation, modification and characterization, Beilstein J. Org. Chem., 16 (2020) 1188–1202.

[29] I. Izhab, M. Asmadi, N. Aishah, S. Amin, Methane dry reforming using oil palm shell activated carbon supported cobalt catalyst: multiresponse optimization, Int. J. Hydrogen Energy, 46 (2021) 24754–24767.

[30] A. Abdedayem, M. Guiza, A. Ouederni, Copper supported on porous activated carbon obtained by wetness impregnation: effect of preparation conditions on the ozonation catalyst's characteristics, C.R. Chim., 18 (2015) 100–109.

[31] K. Derdour, C. Bouchelta, A. Khorief Naser-Eddine, M.S. Medjram, Removal of Cr(VI) from aqueous solutions by using activated carbon supported iron catalysts as efficient adsorbents, World J. Eng., 15 (2018) 3–13.

[32] L. Ai, M. Li, L. Li, Adsorption of methylene blue from aqueous solution with activated carbon/cobalt ferrite/alginate composite beads: kinetics, isotherms, and thermodynamics, J. Chem. Eng. Data, 56 (2011) 3475–3483.

[33] Z. Yang, Z. Zhao, X. Yang, Z. Ren, Iron-cobalt magnetic activated carbon as an effective adsorbent for the removal of methylene blue and Acid Blue 80, Nano Brief Rep. Rev., 16 (2021) 2150068, doi: 10.1142/S1793292021500685.

[34] W. Yang, H. Chen, X. Han, S. Ding, Y. Shan, Y. Liu, Preparation of magnetic Co-Fe modified porous carbon from agricultural wastes by microwave and steam activation for mercury removal, J. Hazard. Mater., 381 (2020) 120981, doi: 10.1016/j.jhazmat.2019.120981.
[35] S. Akbayrak, Z. Özçifçi, A. Tabak, Activated carbon derived from tea waste: a promising supporting material for metal nanoparticles used as catalysts in hydrolysis of ammonia borane, Biomass Bioenergy, 138 (2020) 105589, doi: 10.1016/j.biombioe.2020.105589.
[36] I. Boughaita, C. Bouchalta, M.S. Medjram, P. Magri, Activated carbon supported cobalt as efficiency adsorbent: application chemical agricultural pollutant 2,4-D herbicide removal from aqueous solution, Orient. J. Chem.: Int. Res. J. Pure Appl. Chem., 33 (2017) 2226–2236.
[37] S.Z. Mohammadi, Z. Darijani, M.A. Karimi, Fast and efficient removal of phenol by magnetic activated carbon-cobalt nanoparticles, J. Alloys Compd., 832 (2020) 154942, doi: 10.1016/j.jallcom.2020.154942.
[38] F. Mechati, C. Bouchelta, M.S. Medjram, R. Benrabaa, N. Ammouchi, Effect of hard and soft structure of different biomasses on the porosity development of activated carbon prepared under N_2/microwave radiations, J. Environ. Chem. Eng., 3 (2015) 1928–1938.
[39] M.A. Ahmad, N. Azreen, A. Puad, O.S. Bello, Kinetic, equilibrium and thermodynamic studies of synthetic dye removal using pomegranate peel activated carbon prepared by microwave-induced KOH activation, Water Resour. Ind., 6 (2014) 18–35.
[40] J.M. Ahmed, S.K. Theydan, Optimization of microwave preparation conditions for activated carbon from *Albizia lebbeck* seed pods for methylene blue dye adsorption, J. Anal. Appl. Pyrolysis, 105 (2014) 199–208.
[41] S. Mallakpour, F. Tabesh, Tragacanth gum-based hydrogel nanocomposites for the adsorption of methylene blue: comparison of linear and non-linear forms of different adsorption isotherm and kinetics models, Int. J. Biol. Macromol., 133 (2019) 754–766.
[42] A.R.P. Hidayat, D.O. Sulistiono, I.K. Murwani, B.F. Endrawati, H. Fansuri, L.L. Zulfa, R. Ediati, Linear and nonlinear isotherm, kinetic and thermodynamic behavior of methyl orange adsorption using modulated Al_2O_3@UiO-66 via acetic acid, J. Environ. Chem. Eng., 9 (2021) 106675, doi: 10.1016/j.jece.2021.106675.
[43] N. Ayawei, A.N. Ebelegi, D. Wankasi, Modelling and Interpretation of adsorption isotherms, J. Chem., 2017 (2017) 3039817, doi: 10.1155/2017/3039817.
[44] N. Bougdah, S. Bousba, Y. Belhocine, N. Messikh, Application of multilayer perceptron network and random forest models for modelling the adsorption of chlorobenzene on a modified bentonite by intercalation with hexadecyltrimethyl ammonium (HDTMA), React. Kinet. Mech. Catal., 135 (2021) 247–270.
[45] N. Azouaou, Z. Sadaoui, A. Djaafri, H. Mokaddem, Adsorption of cadmium from aqueous solution onto untreated coffee grounds: equilibrium, kinetics and thermodynamics, J. Hazard. Mater., 184 (2010) 126–134.
[46] C. Djilani, R. Zaghdoudi, A. Modarressid, M. Rogalskid, F. Djazia, A. Lallame, Elimination of organic micropollutants by adsorption on activated carbon prepared from agricultural waste, Chem. Eng. J., 189–190 (2012) 203–212.
[47] B. Chen, Z. Chen, Sorption of naphthalene and 1-naphthol by biochars of orange peels with different pyrolytic temperatures, Chemosphere, 76 (2009) 127–133.
[48] N. Ghadir, A. Hossein, E. Mohamad, Batch adsorption of cephalexin antibiotic from aqueous solution by walnut shell-based activated carbon, J. Taiwan Inst. Chem. Eng., 58 (2016) 357–365.
[49] O.P. Junior, A.L. Cazetta, R.C. Gomes, É.O. Barizão, I.P.A.F. Souza, A.C. Martins, T. Asefa, V.C. Almeida, Synthesis of $ZnCl_2$-activated carbon from macadamia nut endocarp (*Macadamia integrifolia*) by microwave-assisted pyrolysis: optimization using RSM and methylene blue adsorption, J. Anal. Appl. Pyrolysis, 105 (2014) 166–176.
[50] A.H. Jawad, A.S. Abdulhameed, L.D. Wilson, S. Shatir, A. Syed-Hassan, Z.A. ALOthman, M.R. Khan, High surface area and mesoporous activated carbon from KOH-activated dragon fruit peels for methylene blue dye adsorption: optimization and mechanism study, **Chin. J. Chem. Eng.,** 32 (2021) 281–290.
[51] R. Md Salim, J. Asik, M.S. Sarjadi, Chemical functional groups of extractives, cellulose and lignin extracted from native *Leucaena leucocephala* bark, Wood Sci. Technol., 55 (2021) 295–313.
[52] M.A. Ahmad, M.A. Eusoff, P.O. Oladoye, K.A. Adegoke, O.S. Bello, Statistical optimization of Remazol Brilliant Blue R dye adsorption onto activated carbon prepared from pomegranate fruit peel, Chem. Data Collect., 28 (2020) 100426, doi: 10.1016/j.cdc.2020.100426.
[53] J. Srenscek-Nazzal, A. Kamińska, P. Miądlicki, A. Wróblewska, K. Kiełbasa, R.J. Wróbel, J. Serafin, B. Michalkiewicz, Activated carbon modification towards efficient catalyst for high value-added products synthesis from alpha-pinene, Materials, 14 (2021) 7811, doi: 10.3390/ma14247811.
[54] S.A. Kosa, G. Al-Zhrania, S.M. Abdel, Removal of heavy metals from aqueous solutions by multi-walled carbon nanotubes modified with 8-hydroxyquinoline, Chem. Eng. J., 181–182 (2012) 159–168.
[55] T.A. Khan, S.A. Chaudhry, I. Ali, Equilibrium uptake, isotherm and kinetic studies of Cd(II) adsorption onto iron oxide activated red mud from aqueous solution, J. Mol. Liq., 202 (2015) 165–175.
[56] Y.C. Sharma, Uma, S.N. Upadhyay, An economically viable removal of methylene blue by adsorption on activated carbon prepared from rice husk, Can. J. Chem. Eng., 89 (2011) 377–383.
[57] E. Misran, O. Bani, E.M. Situmeang, A.S. Purba, Banana stem based activated carbon as a low-cost adsorbent for methylene blue removal: Isotherm, kinetics, and reusability, Alexandria Eng. J., 61 (2022) 1946–1955.
[58] M. Gouamid, M.R. Ouahrani, M.B. Bensaci, Adsorption equilibrium, kinetics and thermodynamics of methylene blue from aqueous solutions using Date Palm leaves, Energy Procedia, 36 (2013) 898–907.
[59] A.I. Abd-Elhamid, H.F. Aly, H.A.M. Soliman, A.A. El-Shanshory, Graphene oxide: follow the oxidation mechanism and its application in water treatment, J. Mol. Liq., 265 (2018) 226–237.
[60] A. El Amri, J. Bensalah, A. Idrissi, K. Lamya, A. Ouass, S. Bouzakraoui, A. Zarrouk, E. Rifi, A. Lebkiri, Adsorption of a cationic dye (methylene blue) by *Typha Latifolia*: equilibrium, kinetic, thermodynamic and DFT calculations, Chem. Data Collect., 38 (2022) 100834, doi: 10.1016/j.cdc.2022.100834.
[61] G.B. Kankılıc, A.Ü. Metin, I. Tüzün, *Phragmites australis*: an alternative biosorbent for basic dye removal, J. Ecol. Eng., 86 (2016) 85–94.
[62] B. Belhamdi, Z. Merzougui, M. Trari, A. Addoun, A kinetic, equilibrium and thermodynamic study of L-phenylalanine adsorption using activated carbon based on agricultural waste (date stones), J. Appl. Res. Technol., 14 (2016) 354–366.
[63] N.I.I. Zamri, S.L.N. Zulmajdi, N.Z.A. Daud, N.Z.A. Daud, A.H. Mahadi, E. Kusrini, A. Usman, Insight into the adsorption kinetics, mechanism, and thermodynamics of methylene blue from aqueous solution onto pectin-alginate-titania composite microparticles, SN Appl. Sci., 3 (2021) 222, doi: 10.1007/s42452-021-04245-9.
[64] T.S. Anirudhan, M. Ramachandran, Adsorptive removal of tannin from aqueous solutions by cationic surfactant-modified bentonite clay, J. Colloid Interface Sci., 299 (2006) 116–124.
[65] A.M. Chayida, M.J. Ahmed, Amoxicillin adsorption on microwave prepared activated carbon from *Arundo donax* Linn: Isotherms, kinetics, and thermodynamics studies, J. Environ. Chem. Eng., 3 (2015) 1592–1601.
[66] T. Akar, A.S. Ozcan, S. Tunali, A. Ozcan, Biosorption of a textile dye (Acid Blue 40) by cone biomass of *Thuja orientalis*: estimation of equilibrium, thermodynamic and kinetic parameters, Bioresour. Technol., 99 (2008) 3057–3065.
[67] M. Dogan, H. Abak, M. Alkan, Adsorption of methylene blue onto hazelnut shell: kinetics, mechanism and activation parameters, J. Hazard. Mater., 164 (2009) 172–181.

[68] K.L. Tan, B.H. Hameed, Insight into the adsorption kinetics models for the removal of contaminants from aqueous solutions, J. Taiwan Inst. Chem. Eng., 74 (2017) 25–48.
[69] R. Elmoubarki, Adsorption of textile dyes on raw and decanted Moroccan clays: kinetics, equilibrium and thermodynamics, Water Resour. Ind., 9 (2015) 16–29.
[70] X. Tao, Y. Wu, Y. Wu, B. Zhang, H. Sha, L. Cha, N. Liu, Activated carbon-supported cobalt molybdate as a heterogeneous catalyst to activate peroxymonosulfate for removal of organic dyes, Appl. Organomet. Chem., 32 (2018) e4572, doi: 10.1002/aoc.4572.
[71] H.N. Tran, Y.F. Wang, S.J. You, H.P. Chao, Insights into the mechanism of cationic dye adsorption on activated charcoal: the importance of π–π interactions, Process Saf. Environ. Prot., 107 (2017) 168–180.